Biphasic rate exchange in supercooled o-terphenyl from an ensemble analysis of single-molecule data

Harveen Kaur, Sachin Dev Verma, Keewook Paeng, Laura J. Kaufman, and Mark A. Berg

Phys. Rev. E **98**, 040603 — Published 31 October 2018

DOI: 10.1103/PhysRevE.98.040603

Biphasic Rate Exchange in Supercooled *o*-Terphenyl from an Ensemble Analysis of Single-Molecule Data

Harveen Kaur,[1] Sachin Dev Verma,[1] Keewook Paeng,[2,3] Laura J. Kaufman,[2,†] and Mark A. Berg[1,*]

[1]*Department of Chemistry and Biochemistry, University of South Carolina, Columbia, SC 29208, USA*

[2]*Department of Chemistry, Columbia University, New York, NY 10027, USA*

[3]*Department of Chemistry, Sungkyunkwan University, Suwon 16419, Korea*

(Revised, 10/4/2018)

Heterogeneity in relaxation rates is a key feature of supercooled liquids. It implies the existence of a rate-exchange process to restore ergodicity, but the experimental characterization of that exchange has been incomplete and controversial. Here, a recently proposed, ensemble-based analysis is applied to single-molecule dichroism data to extract a detailed correlation function for rotational-rate exchange. A large, late phase is 8.7±0.3 times slower than the probe rotation and 22 times the alpha relaxation time, and it has its own exchange-rate dispersion. A small, early phase tracks the initial rotational decay. We propose that the late phase is due to molecules in the core of spatial regions of correlated rates and that the early phase is due to molecules on the boundaries. The results imply that multiple processes and spatial fields are involved in the primary relaxation in supercooled liquids.

*berg@sc.edu

†kaufman@chem.columbia.edu

Rate dispersion (nonexponential relaxation) is a universal feature of supercooled liquids. Rate heterogeneity is widely accepted to be the dominant mechanism causing this dispersion [1]. Knowing how these heterogeneities evolve to yield a homogeneous, ergodic system at long times is essential for understanding the dynamics leading to the glass transition. Nonetheless, despite nearly three decades of study by a variety of experimental approaches—multidimensional NMR [2-13], deep photobleaching [14], probe-size dependent decay shape [15,16], Stokes-shift line shapes [17], and single-molecule [18-22] studies—there is still disagreement about nearly every aspect of rate exchange: its rate relative to alpha relaxation, its temperature dependence, whether fast structural relaxation correlates with fast exchange, and the extent of rate dispersion in the exchange itself.

Single-molecule dichroism measurements, which monitor the rotation of a probe molecule in a supercooled matrix, have long promised to be a general and direct approach to this problem [18-22]. However, they have been hampered by several problems. First, conventional probe molecules rotate too slowly relative to exchange [15,16,23,24]. Second, photobleaching of the probe molecule limits the dynamic range in time: low light intensities extend the time window, but also require larger time bins to collect sufficient signal. Last and most disturbing, sampling noise—noise due to measuring a finite number of relaxations—is large and has seemed to be unavoidable [25-28].

One of us recently identified the cause of the sampling-noise problem [29]. Conventional analysis of single-molecule kinetics rejects full ensemble averaging in favor of time averages of individual molecules. Although such a molecule-by-molecule analysis is correct for a static heterogeneity, problems arise for systems undergoing exchange. These systems are ergodic; averages over molecules and over time are equivalent. Dropping the average over molecules cannot increase the information content of the measurement; it can only increase noise.

The result is an apparent paradox in which exchange seems to be unmeasurable, even when it is physically relevant. Without an average over molecules, sampling noise is approximately the square root of the number of rotations during the averaging time [30]. However, the

averaging time must be less than the exchange time, leaving an unavoidable amount of sampling noise in a single-molecule average. Thus, molecule-by-molecule averaging does not produce erroneous results, but the correct results become increasingly obscured as the exchange becomes more rapid. Measurements of exchange rates within an order-of-magnitude of the rotation time are impractical; the critical question of whether the rotation rate changes with a single rotation is unanswerable.

The solution to this paradox is to retain full ensemble averages and their low noise, but to average a more complex quantity that can probe the heterogeneity of the system. More specifically, multidimensional correlation functions should be used. A multidimensional analysis of single-molecule dichroism data from the vanden Bout group introduced this idea and used it to demonstrate the existence of rate heterogeneity [29]. However, that data set did not extend to times long enough to measure rate exchange. About the same time, another of us developed a small, fast rotating probe molecule (BODIPY268). With this probe, rate exchange became evident in single-molecule data, even using molecule-by-molecule analysis [31]. New theoretical work has discovered a "rate filtering" term [32] that was not accounted for in previous applications of 3D correlation functions [33-48] (see Supplemental Material (SM) [49]). Methods have been developed to create rate-correlation spectra, to use them to separate rate-filtering from rate-exchange effects [50], to apply these theoretical ideas to real, experimental data, and to combine data sets with different time resolutions and ranges [51]. This Communication combines all these recent advances for the first time to give a quantitative measurement of rate exchange near the glass transition.

In a dichroism experiment, a single molecule is excited with unpolarized light. The fluorescence intensities along two perpendicular polarizations, $I_1(t)$ and $I_2(t)$, are measured as a function of time t. The linear dichroism,

$$D(t) = \frac{I_1(t) - I_2(t)}{I_1(t) + I_2(t)} , \tag{1}$$

fluctuates as the molecule rotates, and an analysis of the resulting trajectories yields the rotational dynamics of the probe. Dichroism dynamics are predominantly those of the second Legendre polynomial of the angle, although a variety of factors can cause small deviations from this ideal [52-54]. (These deviations bring in faster, higher Legendre polynomials and would be detected as homogeneous contributions to the rate dispersion in our multidimensional analysis.)

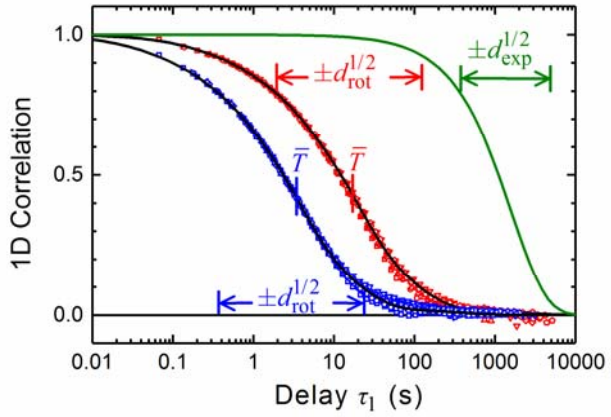

FIG. 1. The 1D correlation function $C_{\rm rot}^{(1)}(\tau_1)$ at two temperatures, 247.5 K (T_g + 4.5 K, blue) and 244.5 K (T_g + 1.5 K, red). Data (points) with different time ranges and resolutions are combined at each temperature ([51] and SM [49]). The black curves are a global fit to both temperatures, assuming time–temperature superposition. The geometric-mean times, $\bar{T}_{\rm rot}$ = 15.6 s or 3.0 s, and total dispersion, $d_{\rm rot}$ = 4.3, are indicated for each temperature. A single-exponential decay, with an arbitrary decay time, is shown for comparison (green, $d_{\rm exp}$ = 1.645).

The standard rotational decay comes from the 1D correlation function,

$$C_{\rm rot}^{(1)}(\tau_1) = \left\langle D(\tau_1)D(0)\right\rangle \Big/ \left\langle D^2 \right\rangle \ , \tag{2}$$

where the brackets indicate a full ensemble average, over both time and molecules. This quantity is shown for two temperatures as the red and blue symbols in Fig. 1. As expected,

time–temperature superposition works well over this small temperature range. Figure 1 shows a fit to a common decay shape with a 5.2-fold time shift between the two temperatures (SM [49]).

The 1D results are conventional, but they are described here by quantities that have been specifically designed to facilitate multidimensional analysis. The time decay is converted to a "decay spectrum",

$$\hat{C}^{(1)}_{\mathrm{rot}}\left(\ln\frac{T_1}{\overline{T}_{\mathrm{rot}}}\right)=\left[\frac{\partial C^{(1)}_{\mathrm{rot}}(\tau_1)}{\partial\ln\left(\tau_1/\overline{T}_{\mathrm{rot}}\right)}\right]_{\tau_1=T_1}, \tag{3}$$

which is a peaked function. Its first moment is the geometric-mean time $\overline{T}_{\mathrm{rot}}$ of the time decay and is similar to its half-life. The variance of the decay spectrum, the total dispersion d_{rot}, measures the spread of the decay in time. Its square root is similar to the time from the half-life to the quarter-life, in factors of e (Fig. 1). For reference, the dispersion measured here, $d_{\mathrm{rot}} = 4.3$, corresponds to $\beta = 0.62$ in a stretched exponential, $\exp[-(\tau/T_{\mathrm{st}})^{\beta}]$. For more detail, see Ref. [50] and SM [49].

The total dispersion d_{rot} consists of a contribution from the expected exponential decay d_{exp} and an excess dispersion, which consists of homogeneous d_{hom} and heterogeneous d_{het} contributions. The heterogeneous dispersion is the variance of the distribution of time constants on a log-time scale. The excess homogeneous dispersion is identical to the variance of an inverse-Laplace transform of the decay, again calculated on a log-time scale. In the case of a slowly varying heterogeneity, the decay spectrum is a convolution of spectra corresponding to each source of dispersion, and the variances are additive [50],

$$d_{\mathrm{rot}} = d_{\mathrm{hom}} + d_{\mathrm{exp}} + d_{\mathrm{het}} \ . \tag{4}$$

The different contributions to the total dispersion are disentangled by the 3D correlation function,

$$C^{(3)}_{\mathrm{rot}}(\tau_3,\tau_2,\tau_1)=\left\langle D(\tau_3+\tau_2+\tau_1)D(\tau_2+\tau_1)D(\tau_1)D(0)\right\rangle\Big/\left\langle D^4\right\rangle \ . \tag{5}$$

Notice that all four measurements in the average must come from the same molecule and that the average is still over both molecules and time. Thus, the 3D correlation function is an ensemble measurement, but it requires single-molecule data.

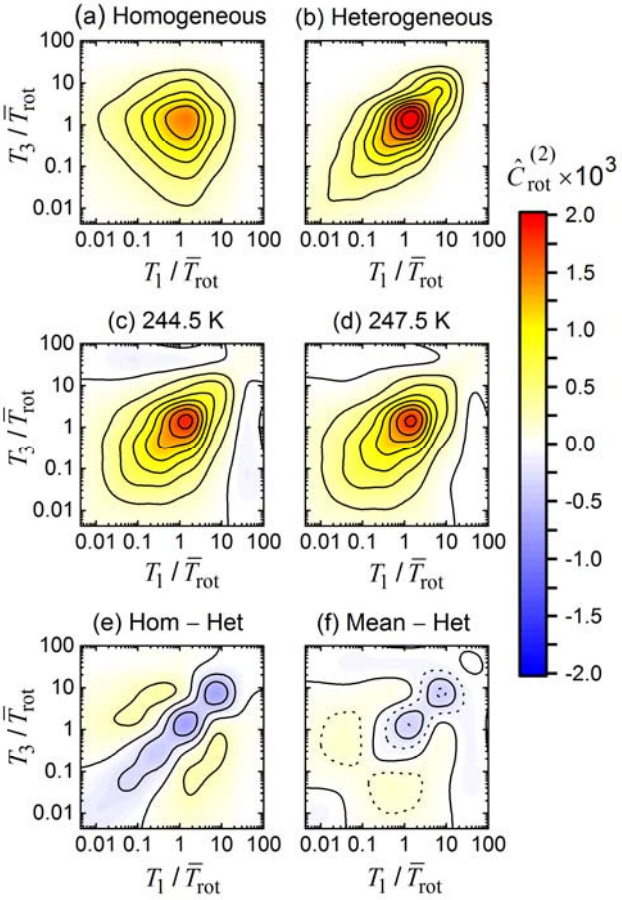

FIG. 2. 2D correlation function as decay spectra $\hat{C}^{(2)}_{\rm rot}(T_3, T_1)$. Predictions for (a) pure homogeneous dispersion and (b) pure heterogeneous dispersion (SM [49]). (c & d) Spectra from the dichroism data at two temperatures. (e) The difference between the predictions, (b) and (a). (f) The difference between the mean of the data (c & d) and the heterogeneous prediction (ab). Solid contours are at the ticks on the legends. Dotted contours are at half the spacing of the full contours.

The multidimensional analysis begins with the $\tau_2 = 0$ slice of this function. It is converted to the 2D decay spectrum [50], which is shown in Figs. 2(c) and 2(d). These spectra show the correlation between two time constants, T_1 and T_3. (Because a logarithmic scale is used, rates and time constants are equivalent. They only differ by a sign.) Every time constant correlates with itself, so there is always intensity along the diagonal. Greater dispersion implies a broader range of time constants and an increased spread along the diagonal. If the kinetics are homogeneous, every time constant in the sample occurs on the same molecule as part of the same kinetic scheme, and thus, each time constant correlates with every other time constant. Off-diagonal intensity is strong, so the spectrum is compact [Fig. 2(a)]. On the other hand, if the kinetics are heterogeneous, different time constants occur on different molecules and do not correlate. Off-diagonal intensity is weak, and the spectrum is elongated [Fig. 2(b)].

The spectra calculated from the data are shown in Figs. 2(c) and 2(d). The two data sets have been analyzed, fit and transformed independently ([51] and SM [49]). After correcting for the time shift, as measured by the 1D data, the two spectra are nearly identical: the 2D correlation functions obey time–temperature superposition. We do not believe the small differences between the spectra are real; they represent experimental error.

The spectra in Figs. 2(c) and 2(d) are elongated along the diagonal, and thus, strong rate heterogeneity is present. However, the spectra are not as elongated as the prediction based on heterogeneous dispersion alone [Fig. 2(b)]. The variances of the projections of the spectrum along the diagonal and antidiagonal are used to calculate f_{het}, which quantifies the location of the real spectra between the predicted limits ([50] and SM [49]). Within a model based on slow exchange, this parameter gives the fraction of the excess rate dispersion due to heterogeneous processes,

$$f_{\text{het}} = \frac{d_{\text{het}}}{d_{\text{hom}} + d_{\text{het}}}, \tag{6}$$

It is found to be f_{het} = 0.65±0.02 (mean of both temperatures with their range as the error estimate), suggesting a significant source of homogeneous dispersion.

The slow-exchange model also predicts that the off-diagonal intensity, which is associated with the purported homogeneous process, will be distributed uniformly across all time constants. Figure 2(e) highlights the predicted distribution by subtracting the diagonal, heterogeneous spectra from the homogeneous spectrum. In this model calculation, the positive (yellow) off-diagonal intensity is spread evenly along the diagonal. In Fig. 2(f), the heterogeneous prediction is subtracted from the mean of the two experimental spectra. The positive intensity is focused on the early part of the decay, a deviation from the slow-heterogeneity model prediction [Fig. 2(e)]. We will argue below that both the below unity value of f_{het} and the uneven distribution of off-diagonal intensity are not due to a homogenous source of rate dispersion, but rather are due to a subset of molecules that lie outside the slow-exchange limit.

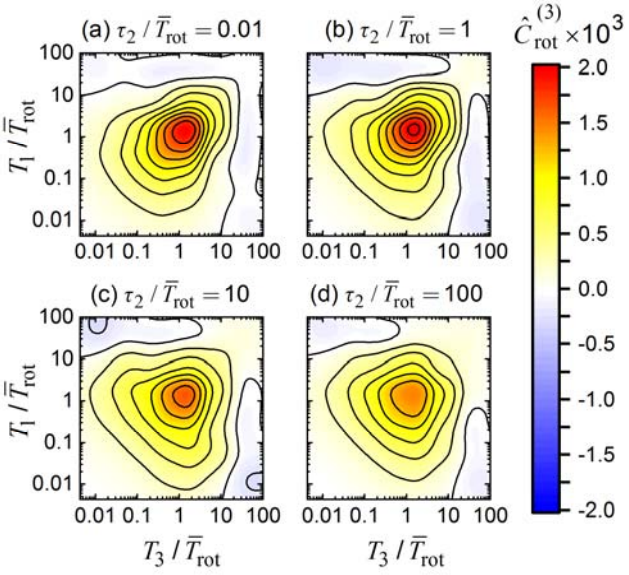

FIG. 3. 3D correlation function $\hat{C}^{(3)}_{rot}(T_3, \tau_2, T_1)$. The average of the two temperatures is shown. Each panel is normalized to unit volume.

The full 3D correlation function is calculated from Eq. (5) using all points with $\tau_2 > 0$. (Because the $\tau_2 = 0$ points contain an extra contribution from detector noise, they are only used in the 2D correlation [51].) The 3D function is presented as a series of slices at fixed τ_2, each of which has been transformed to a 2D spectrum $\hat{C}^{(3)}_{\mathrm{rot}}(T_3,\tau_2,T_1)$ [50]. The results for each temperature are very similar (SM [49]), that is, time–temperature superposition holds again. The mean of the two temperatures is shown in Fig. 3.

The evolution along τ_2 is sensitive to rate exchange. If a molecule has a time constant T_1 during τ_1, but exchanges to T_3 during τ_2, those time constants will become correlated. As exchange proceeds, off-diagonal intensity will build, broadening the spectrum in the antidiagonal direction and shrinking it along the diagonal [50]. This process is visible in Fig. 3, showing that exchange is occurring. For τ_2 longer than the exchange time, the 3D spectrum should look like a fully homogeneous 2D spectrum. The predicted homogeneous spectrum [Fig. 2(a)] and observed 3D spectrum at long τ_2 [Fig. 3(d)] are quite similar, showing that the time range of the data fully captures the exchange.

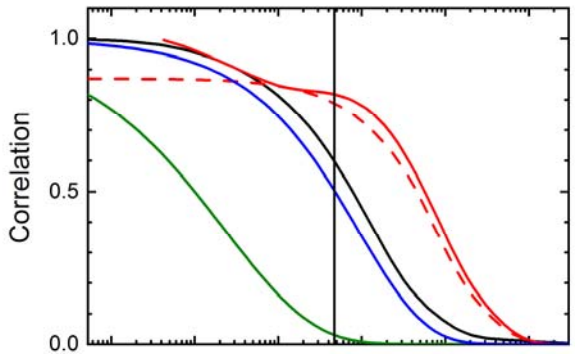

FIG. 4. The apparent heterogeneity $f_{\rm het}(\tau_2)$ (solid red) extracted from the 3D correlation data (Fig. 3) compared to other relaxations. The late phase of exchange has been separated and corrected for deviations from the slow-heterogeneity limit to give the correlation function of the molecular time constant $C_{\rm ex}^{(1)}(\tau_2)$ [dashed red, Eq. (7)]. The 1D correlation functions for full rotation (black, fit from Fig. 1), for dielectric alpha relaxation (blue) [55], and for orientational jumps (green) [11]are shown for comparison. The vertical line marks the 90% point of $C_{\rm ex}^{(1)}(\tau_2)$. Earlier times are minimally affected by late-phase rate exchange, but may be affected by the early phase.

The exchange is quantified by calculating the apparent heterogeneity as a function of time $f_{\rm het}(\tau_2)$ (SM [49]). The result is shown as the red curve in Fig. 4. The exchange occurs in two phases, an early phase for $\tau_2 \lesssim 0.1\ \overline{T}_{\rm rot}$ and a late phase for $\tau_2 \gtrsim \overline{T}_{\rm rot}$.

The parameter $f_{\rm het}(\tau_2)$ has been designed to eliminate contributions from rate-filtering during τ_2 in the limit of slow exchange, $\overline{T}_{\rm ex} \gg \overline{T}_{\rm rot}$ [50]. The late phase of $f_{\rm het}(\tau_2)$ has been separated and corrected for the residual rate-filtering effect [50] to give $C_{\rm ex}^{(1)}(\tau_2)$ (Fig. 4, red, dashed curve). This function can be quantitatively interpreted as the 1D correlation of the time-dependent time constant for a specific molecule $T_{\rm rot}(\tau_2)$:

$$C_{\rm ex}^{(1)}(\tau_2) = \left\langle \ln\frac{T_{\rm rot}(\tau_2)}{\overline{T}_{\rm rot}} \ln\frac{T_{\rm rot}(0)}{\overline{T}_{\rm rot}} \right\rangle \Bigg/ \left\langle \left(\ln\frac{T_{\rm rot}}{\overline{T}_{\rm rot}} \right)^2 \right\rangle . \qquad (7)$$

The geometric-mean time of the late phase of exchange is $\overline{T}_{ex} = 8.7 \pm 0.3\ \overline{T}_{rot}$. The rotation time of our dye is slightly longer than the dielectric alpha-relaxation time $\overline{T}_{\alpha}$, due differences in the sizes of the probe and *o*-terphenyl molecules and due to differences in the Legendre polynomial P_n measured by optical (P_2) and dielectric (P_1) experiments [56]. Measurements show that $\overline{T}_{rot} = 2.5\ \overline{T}_{\alpha}$ [31], which gives $\overline{T}_{ex} = 22\ \overline{T}_{\alpha}$. The late phase of exchange is not exponential, but rather, it has an excess exchange-rate dispersion of $d_{ex} = 1.23 \pm 0.05$ ($\beta = 0.76$). A nonexponential exchange indicates that there is yet another process with a similar or longer relaxation time that holds memory of the exchange rate.

The early phase of $f_{het}(\tau_2)$ decays in concert with $C_{rot}^{(1)}(\tau_1)$. This phase is close to the intermediate-exchange case, $\overline{T}_{ex} = \overline{T}_{rot}$, for which the theory of multidimensional correlation functions is less well developed. As a result, the early phase of $f_{het}(\tau_2)$ must be interpreted more qualitatively. If a molecule retains its rotation rate for two rotations, one during τ_1 and another during τ_2, it will appear heterogeneous. If a molecule retains memory of its rotation rate for one rotation, but not two, it will contribute to dispersion in the 1D decay, but it will not appear to be heterogeneous in a multidimensional measurement. In other words, the intermediate-exchange molecule will appear to have homogeneous dispersion. In an ensemble with intermediate-exchange heterogeneity, a combination of these effects would occur: apparently homogeneous dispersion along with rapidly decaying $f_{het}(\tau_2)$. Thus, a single subset of molecules with intermediate exchange rates would account for the high off-diagonal intensity and the apparently low heterogeneity in the 2D measurements and for the early phase of $f_{het}(\tau_2)$ in the 3D measurements. Both the 2D and 3D measurements show that these intermediate-exchange molecules are concentrated in the fast part of the rotational-rate distribution.

Rate heterogeneity occurs in well-defined spatial regions [1]. These domains provides a plausible explanation for the biphasic exchange. Molecules in the bulk of the domains rotate slowly and exchange even more slowly. The boundaries between domains have less stable local configurations, so molecules in them rotate rapidly and exchange just as quickly. In this

interpretation, the early and late phases of exchange represent boundary and bulk molecules, respectively.

Previous reports of exchange dynamics have given a variety of results, ranging from much faster to much slower than the current value. The analysis of very similar single-molecule data with molecule-by-molecule methods identified the slower exchange components seen here, but not the faster ones [31]. This result is consistent with the expectation that molecule-by-molecule methods will have greater problems identifying faster exchange times [28,29]. Studies of rotational-rate dispersion versus probe size reported $\overline{T}_{\mathrm{ex}} \sim 2\ \overline{T}_{\alpha}$ [16], ten times faster than our result of $\overline{T}_{\mathrm{ex}} = 22\ \overline{T}_{\alpha}$. Studies of solvation line shapes [17] and of solvation-rate dispersion versus probe size [15] indicated that exchange is more than 9 or more than 20 times slower than solvation, respectively. The interpretation of the solvation results depends on whether the solvation time is the same as the alpha-relaxation time [57] or ten times faster [16]. NMR experiments reported exchange in the rate of orientational jumps $\overline{T}_{\mathrm{jmp}}$ rather than in the rate of full rotation (SM [49]) [2-13]. In *o*-terphenyl, they found a range of exchange times spreading over a decade in time and centered near $\overline{T}_{\mathrm{ex}} \sim 0.3\ \overline{T}_{\alpha}$ [11]. Although there is some overlap, most of their reported exchange is faster than ours. (Because the fast-exchange components, those with $\overline{T}_{\mathrm{ex}} < \overline{T}_{\mathrm{rot}}$, would not contribute to the rate dispersion of the full rotation, it is not clear whether the NMR results are compatible with the strong rate dispersion seen in the 1D rotational decay.) Deep photobleach experiments reported power-law exchange decays extending to hundreds of times the alpha-relaxation time [14]. They also found that the exchange rate changes with temperature much more rapidly than expected from time–temperature superposition. Both of these results disagree with ours.

Two limiting cases help to guide the interpretation of our results: exchange is either simultaneous with the primary structural relaxation of the liquid or quasi-static with respect to it. Which limit is more correct depends on which phase of exchange and which aspect of structural relaxation we consider.

Relaxation occurs through a sequence of jumps, each small relative to a molecular dimension. These jumps are arguably the fundamental reorganization event that drives relaxation, in which case, rate exchange is equivalent to a change in jump rate. In the case of rotation, NMR measurements indicate a jump angle of ~10° in *o*-terphenyl [58]. A simple model [59] and the measured jump angle give the P_1-rotation time as $\overline{T}_\alpha = 66\ \overline{T}_{\rm jmp}$. Thus, $\overline{T}_{\rm ex} \approx 1.4\times10^3\ \overline{T}_{\rm jmp}$. On average, molecules in the bulk of the domains undergo thousands of jumps before changing their rate. Figure 4 shows the jump-correlation function from NMR [11] along with the exchange-correlation function. The jump correlation has completely decayed before late-phase exchange begins. For molecules in the bulk of the domains, even the slowest orientational jumps occur with a quasi-static jump rate.

However, the early phase of exchange does overlaps the jump-correlation function in time. Because the effects of exchange become averaged as the exchange become faster than rotation, it is possible that this phase is somewhat faster and larger than it appears. For molecules in the domain boundaries, jumps and exchange could be nearly simultaneous. The structural reorganization associated with a single jump might strongly affect the rate of the next jump.

Multiple small jumps eventually lead to motion on a molecular dimension. For example, the dielectric alpha-relaxation time $\overline{T}_\alpha$ measures reorientation of the host molecule over ~180°. Comparing mean times, $\overline{T}_{\rm ex} = 22\ \overline{T}_\alpha$, shows that most *o*-terphenyl molecules make many full rotations before rate exchange occurs.

However, the rates of rotation and of exchange are distributed, and mean times may not capture the complete story. The full dielectric alpha-relaxation function [55] has been plotted in Fig. 4. The vertical line approximately separates time regions where late-phase exchange is and is not important. The tail of the alpha relaxation falls in a region where exchange is beginning to be active.

This result relates to a common observation. When stretched relaxations are expressed as a distribution of rates, the distribution typically has a long tail for fast rates, but a sharp cut-off for slow rates. For example, stretched exponentials have this type of distribution. It has been

hypothesized that rate distributions are intrinsically more symmetric, but that very slow rotation is disrupted by exchange to a faster rate [1,60]. Looking at the region affected by exchange in Fig. 4, this scenario may apply, and a subset of slow molecules may have their rotation affected by exchange.

To summarize, for the majority of molecules, rate exchange is slow compared to structural relaxation. However, subsets of molecules that are in the boundaries of domains or that are in the tail of the rate distribution might exchange in as little as one relaxation event. The size of these subsets will vary with the mean time and dispersion of the particular process being considered.

The overall slowness of exchange is not compatible with theories that have structural relaxation and exchange coming from the same mechanism. An example is the Random First-Order Transition (RFOT) explanation for rate heterogeneity [60]. In this theory, a mosaic of "phase droplets" defines both the local structure and the local relaxation rate. Nucleation and growth of a new droplet changes both. Whether this event is associated with a single reorganizational jump or with alpha relaxation, exchange should be simultaneous with relaxation. The exchange rate we find is too slow for this prediction.

Our explanation for biphasic exchange is based on spatial domains defined as a group of molecules with a common alpha-relaxation rate. The exchange rate is the lifetime of these domains. In other discussions, a domain is defined as a cluster of molecules undergoing cooperative motion [61]. If structural relaxation and exchange are simultaneous, this distinction is unimportant, and only one type of spatial domain exists. In the RFOT example, a phase droplet defines the spatial range of both cooperative reorganization and common relaxation rate. However, if slow exchange implies that there are different processes for relaxation and exchange, there may be different spatial domains connected with each process.

In summary, an ensemble-based approach to analyzing single-molecule data allows rate exchange to be measured with quantitative accuracy. The observation of two phases in the exchange decay is consistent with the common, domain picture of supercooled liquids, with the

late and early phases of exchange assigned to the bulk and boundaries of the domains, respectively. The slowness and nonexponential relaxation of the bulk exchange show that full equilibration of supercooled liquids requires process beyond those creating alpha relaxation. Single-molecule measurements can now provide the experimental data needed to study those processes.

ACKNOWLEDGEMENTS

This material is based upon work supported by the National Science Foundation under Grant Nos. CHE-1403027 and CHE-1707813 to MAB and CHE-1213242 and CHE-1660392 to LJK.

REFERENCES

[1] L. Berthier, G. Biroli, J.-P. Bouchaud, L. Cipelletti, and W. van Saarloos, *Dynamical heterogeneities in glasses, colloids and granular media* (Oxford University Press, Oxford, 2011), p. 480.

[2] K. Schmidt-Rohr and H. W. Spiess, Nature of nonexponential loss of correlation above the glass transition investigated by multidimensional NMR, Phys. Rev. Lett. **66**, 3020 (1991).

[3] A. Heuer, M. Wilhelm, H. Zimmermann, and H. W. Spiess, Rate memory of structural relaxation in glasses and its detection by multidimensional NMR, Phys. Rev. Lett. **75**, 2851 (1995).

[4] A. Heuer, Information content of multitime correlation functions for the interpretation of structural relaxation in glass-forming systems, Phys. Rev. E **56**, 730 (1997).

[5] S. C. Kuebler, A. Heuer, and H. W. Spiess, Glass transition of polymers: Memory effects in structural relaxation of polystyrene, Phys. Rev. E **56**, 741 (1997).

[6] U. Tracht, M. Wilhelm, A. Heuer, H. Feng, K. Schmidt-Rohr, and H. W. Spiess, Length scale of dynamic heterogeneities at the glass transition determined by multidimensional nuclear magnetic resonance, Phys. Rev. Lett. **81**, 2727 (1998).

[7] U. Tracht, A. Heuer, and H. W. Spiess, Different dynamic filters constructed from multidimensional NMR experiments, J. Non-Cryst. Solids **235-237**, 27 (1998).

[8] U. Tracht, A. Heuer, S. A. Reinsberg, and H. W. Spiess, The rate memory of a polymer close to T_g as elucidated by reduced 4-D NMR echo experiments, Appl. Magn. Reson. **17**, 227 (1999).

[9] F. Fujara, B. Geil, H. Sillescu, and G. Fleischer, Translational and rotational diffusion in supercooled orthoterphenyl close to the glass transition, Z. Physik B - Condensed Matter **88**, 195 (1992).

[10] R. Böhmer, G. Hinze, G. Diezemann, B. Geil, and H. Sillescu, Dynamic heterogeneity in supercooled ortho-terphenyl studied by multidimensional deuteron NMR, Europhys. Lett. **36**, 55 (1996).

[11] R. Böhmer, G. Diezemann, G. Hinze, and H. Sillescu, A nuclear magnetic resonance study of higher-order correlation functions in supercooled ortho-terphenyl, J. Chem. Phys. **108**, 890 (1998).

[12] F. Qi *et al.*, Nuclear magnetic resonance and dielectric spectroscopy of a simple supercooled liquid: 2-methyl tetrahydrofuran, J. Chem. Phys. **118**, 7431 (2003).

[13] G. Hinze, Geometry and time scale of the rotational dynamics in supercooled toluene, Phys. Rev. E **57**, 2010 (1998).

[14] C. Y. Wang and M. D. Ediger, How long do regions of different dynamics persist in supercooled *o*-terphenyl?, J. Phys. Chem. B **103**, 4177 (1999).

[15] L.-M. Wang and R. Richert, Exponential probe rotation in glass-forming liquids, J. Chem. Phys. **120**, 11082 (2004).

[16] W. Huang and R. Richert, From heterogeneous probe rotation to the hydrodynamic limit, J. Non-Cryst. Solids **352**, 4704 (2006).

[17] R. Richert, Spectral diffusion in liquids with fluctuating solvent responses: Dynamical heterogeneity and rate exchange, J. Chem. Phys. **115**, 1429 (2001).

[18] L. A. Deschenes and D. A. Vanden Bout, Heterogeneous dynamics and domains in supercooled *o*-terphenyl: A single molecule study, J. Phys. Chem. B **106**, 11438 (2002).

[19] R. Zondervan, F. Kulzer, G. C. G. Berkhout, and M. Orrit, Local viscosity of supercooled glycerol near T_g probed by rotational diffusion of ensembles and single dye molecules, Proc. Natl. Acad. Sci. U.S.A. **104**, 12628 (2007).

[20] S. A. Mackowiak, T. K. Herman, and L. J. Kaufman, Spatial and temporal heterogeneity in supercooled glycerol: Evidence from wide field single molecule imaging, J. Chem. Phys. **131**, 244513 (2009).

[21] L. J. Kaufman, Heterogeneity in single-molecule observables in the study of supercooled liquids, Annu. Rev. Phys. Chem. **64**, 177 (2013).

[22] K. Paeng and L. J. Kaufman, Single molecule rotational probing of supercooled liquids, Chem. Soc. Rev. **43**, 977 (2014).

[23] S. A. Mackowiak, L. M. Leone, and L. J. Kaufman, Probe dependence of spatially heterogeneous dynamics in supercooled glycerol as revealed by single molecule microscopy, Phys. Chem. Chem. Phys. **13**, 1786 (2011).

[24] L. M. Leone and L. J. Kaufman, Single molecule probe reports of dynamic heterogeneity in supercooled ortho-terphenyl, J. Chem. Phys. **138**, 12A524 (2013).

[25] C. Y. Lu and D. A. Vanden Bout, Effect of finite trajectory length on the correlation function analysis of single molecule data, J. Chem. Phys. **125**, 124701 (2006).

[26] C.-Y. J. Wei, C.-Y. Lu, Y. H. Kim, and D. A. Vanden Bout, Determining if a system is heterogeneous: The analysis of single molecule rotational correlation functions and their limitations, J. Fluoresc. **17**, 797 (2007).

[27] S. A. Mackowiak and L. J. Kaufman, When the heterogeneous appears homogeneous: Discrepant measures of heterogeneity in single-molecule observables, J. Phys. Chem. Lett. **2**, 438 (2011).

[28] K. Stokely, A. S. Manz, and L. J. Kaufman, Revealing and resolving degeneracies in stretching exponents in temporally heterogeneous environments, J. Chem. Phys. **142**, 114504 (2015).

[29] S. D. Verma, D. A. Vanden Bout, and M. A. Berg, When is a single molecule homogeneous? A multidimensional answer and its application to molecular rotation near the glass transition, J. Chem. Phys. **143**, 024110 (2015).

[30] R. Zwanzig and N. K. Ailawadi, Statistical error due to finite time averaging in computer experiments, Phys. Rev. **182**, 280 (1969).

[31] K. Paeng, H. Park, D. T. Hoang, and L. J. Kaufman, Ideal probe single-molecule experiments reveal the intrinsic dynamic heterogeneity of a supercooled liquid, Proc. Natl. Acad. Sci. U.S.A. **112**, 4952 (2015).

[32] M. A. Berg and J. R. Darvin, Measuring the dynamics of a hidden coordinate: Rate exchange from 3D correlation functions, J. Chem. Phys. **145**, 054119 (2016).

[33] K. Kim and S. Saito, Multiple length and time scales of dynamic heterogeneities in model glass-forming liquids: A systematic analysis of multi-point and multi-time correlations, J. Chem. Phys. **138**, 12A506 (2013).

[34] K. Kim and S. Saito, Hidden slow time scale of correlated motions in supercooled liquids: Multi-time correlation function approach, J. Non-Cryst. Solids **357**, 371 (2011).

[35] K. Kim and S. Saito, Multi-time density correlation functions in glass-forming liquids: Probing dynamical heterogeneity and its lifetime, J. Chem. Phys. **133**, 044511 (2010).

[36] K. Kim and S. Saito, Multiple time scales hidden in heterogeneous dynamics of glass-forming liquids, Phys. Rev. E **79**, 060501 (2009).

[37] J. Ono, S. Takada, and S. Saito, Couplings between hierarchical conformational dynamics from multi-time correlation functions and two-dimensional lifetime spectra: Application to adenylate kinase, J. Chem. Phys. **142**, 212404 (2015).

[38] S. Léonard and L. Berthier, Lifetime of dynamic heterogeneity in strong and fragile kinetically constrained spin models, J. Phys.: Condens. Matter **17**, S3571 (2005).

[39] E. Flenner and G. Szamel, Lifetime of dynamic heterogeneities in a binary lennard-jones mixture, Phys. Rev. E **70**, 052501 (2004).

[40] H. Mizuno and R. Yamamoto, Dynamical heterogeneity in a highly supercooled liquid under a sheared situation, J. Chem. Phys. **136**, 084505 (2012).

[41] H. Mizuno and R. Yamamoto, Dynamical heterogeneity in a highly supercooled liquid: Consistent calculations of correlation length, intensity, and lifetime, Phys. Rev. E **84**, 011506 (2011).

[42] H. Mizuno and R. Yamamoto, Lifetime of dynamical heterogeneity in a highly supercooled liquid, Phys. Rev. E **82**, 030501 (2010).

[43] G. Diezemann, Higher-order correlation functions and nonlinear response functions in a gaussian trap model, J. Chem. Phys. **138**, 12A505 (2013).

[44] R. van Zon and J. Schofield, Mode-coupling theory for multiple-time correlation functions of tagged particle densities and dynamical filters designed for glassy systems, J. Phys. Chem. B **109**, 21425 (2005).

[45] R. van Zon and J. Schofield, Mode-coupling theory for multiple-point and multiple-time correlation functions, Phys. Rev. E **65**, 011106 (2001).

[46] R. van Zon and J. Schofield, Multiple-point and multiple-time correlation functions in a hard-sphere fluid, Phys. Rev. E **65**, 011107 (2001).

[47] B. Doliwa and A. Heuer, Cage effect, local anisotropies, and dynamic heterogeneities at the glass transition: A computer study of hard spheres, Phys. Rev. Lett. **80**, 4915 (1998).

[48] A. Heuer and K. Okun, Heterogeneous and homogeneous dynamics in a simulated polymer melt: Analysis of multi-time correlation functions, J. Chem. Phys. **106**, 6176 (1997).

[49] See Supplemental Material at http://link.aps.org/xxxx for additional information on data reduction methods, error assessment, calculating model spectra, nonparameteric measures of kinetics, differences from previous multidimensional studies and differences from multidimensional NMR experiements.

[50] M. A. Berg and H. Kaur, Non-parametric analysis of nonexponential and multidimensional kinetics: I. Quantifying rate dispersion, heterogeneity and exchange, J. Chem. Phys. **146**, 054104 (2017).

[51] H. Kaur, S. D. Verma, K. Paeng, L. Kaufman, and M. A. Berg, in preparation.

[52] G. Hinze, G. Diezemann, and T. Basché, Rotational correlation functions of single molecules, Phys. Rev. Lett. **93**, 203001 (2004).

[53] C.-Y. J. Wei, Y. H. Kim, R. K. Darst, P. J. Rossky, and D. A. Vanden Bout, Origins of nonexponential decay in single molecule measurements of rotational dynamics, Phys. Rev. Lett. **95**, 173001 (2005).

[54] D. T. Hoang, K. Paeng, H. Park, L. M. Leone, and L. J. Kaufman, Extraction of rotational correlation times from noisy single molecule fluorescence trajectories, Anal. Chem. **86**, 9322 (2014).

[55] R. Richert, On the dielectric susceptibility spectra of supercooled *o*-terphenyl, J. Chem. Phys. **123**, 154502 (2005).

[56] In our comparisons of different experiments, we assume that P_2 relaxation is three times faster than P_1 relaxation and neglect differences between long-wavelength (e.g., dielectric) and single-particle (e.g., probe rotation) measurements.

[57] R. Richert, Triplet state solvation dynamics: Basics and applications, J. Chem. Phys. **113**, 8404 (2000).

[58] B. Geil, F. Fujara, and H. Sillescu, ^{2}H NMR time domain analysis of ultraslow reorientations in supercooled liquids, J. Magn. Reson. **130**, 18 (1998).

[59] J. E. Anderson, Environmental fluctuations and rotational processes in liquids, Faraday Symp. Chem. Soc. **6**, 82 (1972).

[60] X. Xia and P. G. Wolynes, Microscopic theory of heterogeneity and nonexponential relaxation in supercooled liquids, Phys. Rev. Lett. **86**, 5526 (2001).

[61] G. Adam and J. H. Gibbs, On the temperature dependence of cooperative relaxation properties in glass-forming liquids, J. Chem. Phys. **43**, 139 (1965).